



## **Streamlined design of nonprismatic I-section members**

Ryan Slein<sup>1</sup>, Donald W. White<sup>2</sup>

### **Abstract**

In metal building frame design, significant design economy is commonly gained by varying the web depth along I-section member lengths, as well as by stepping the web and flange plate thicknesses, and in some cases the flange widths, at selected positions along the member lengths. Similarly, design economy is achieved in bridge I-girder design by stepping the cross-section geometry at selected positions along the member lengths. In addition, for continuous-span bridge I-girders with spans beyond approximately 200 ft, significant design economies are commonly realized by using a continuously varying web depth, e.g., haunched girders, within negative moment regions. All of these nonprismatic member designs vary the member capacities largely to better fit the required elastic moment envelopes obtained from a structural analysis.

Efficient routine design of nonprismatic I-section members can be achieved by a straightforward adaptation of the AISC (2016) and/or AASHTO (2017) design provisions for prismatic I-section members. This paper first focuses on explaining the theoretical and conceptual basis for these adaptations, which are captured within the *AISC/MBMA Design Guide 25* (2019) recommendations, as well as in draft updates to the AASHTO LRFD rules. Secondly, the paper focuses on the streamlined manual calculation of design quantities, particularly on methods of estimating lateral-torsional-buckling (LTB) resistances for various nonprismatic member geometries. Lastly, the paper compares the resistance predictions to results from experimental tests and test simulations.

### **1. Introduction**

Nonprismatic I-section members are widely employed for optimized design of members subjected predominantly to flexure. For example, the metal building industry often designs frame members with a single or double linear variation in the web depth along the member length. The loads are discretely introduced into the frame through purlins and girts, and the resulting moment diagram is approximately linear between each purlin/girt. Lateral and torsional displacements are typically restrained at certain locations by purlins/girts and by diagonal members framed between the purlins/girts and the bottom or inside flange of the member. Following traditional design checks for the unbraced length that disregard continuity effects, one option is to use prismatic flanges and vary the web depth to follow to moment diagram. Further economy can be gained by using singly

---

<sup>1</sup> Graduate Research Assistant, Georgia Institute of Technology, <ryan.slein@gatech.edu>

<sup>2</sup> Professor, Georgia Institute of Technology, <dwhite@ce.gatech.edu>

symmetric cross-sections that are sized to match the various limit states. This achieves more uniform capacity-to-demand ratios for both flanges along the entire unbraced length. The lateral-torsional-buckling (LTB) capacity of a section can be directly increased by widening or thickening the compression flange. The effective radius of gyration for lateral-torsional-buckling increases approximately in a linear fashion with increases in the compression flange width, which in turn quadratically increases the elastic LTB capacity of the member. Thickening the compression flange has a lesser effect on the effective radius of gyration, but decreases the depth of the web in compression, thus reducing the compression flange stress for a given moment.

Several key stability attributes are introduced when varying the web depth: 1) in most applications, one flange will be parallel to the axis of any torsional restraint and the other flange will follow the taper angle; 2) the shear center height varies relative to the flanges as one moves along the length; and 3) the moment diagram may be nearly linear but in most cases the flange stress diagram is nonlinear. These effects on the member stability are considered in the derivation of the nonprismatic geometry factor ( $\chi$ ) discussed in Section 4 of this paper.

Continuous bridge I-girders typically have regions of smaller positive moment within the span and larger negative moments at the piers. Haunched girders are often utilized to follow the increased demands at the piers. Various equations are used to define the geometric variation in the web depth. If the haunch has a variation in web depth that is concave (e.g. the web depth along the length is more shallow than the chord between the points at the bottom of the web at the start and end of the variation) then the effects on the member stability can be approximated conservatively by treating the member as having a single linear variation in the web depth for calculation of the nonprismatic geometry factor. If the top flange is in compression, the geometry of the bottom flange has little effect on the elastic LTB resistance. If the bottom flange is in compression, a concave parabolic haunch exhibits an “inverted arch effect,” improving the out-of-plane stability characteristics. This approximation is not applicable for a convex (e.g. a “fish belly”) haunch where the member may exhibit an “arch effect.”

Besides varying the web depth, the cross-section geometries are often stepped in both metal buildings and I-girder bridges to achieve a structurally efficient design. (Stepped sections at locations other than field splices often require a justification in material saving to outweigh additional fabrication costs.) Using the method presented in this paper, the capacities for each of the aforementioned nonprismatic geometries, including steps in the cross-section in combination with varying web depth, can be manually estimated through straightforward calculations.

## **2. Background**

Guidance on how to manually estimate the capacity of nonprismatic members in design provisions is very limited. The AISC (2016) *Specification* does not address nonprismatic members at all. Instead, AISC refers users to the first edition of Design Guide 25 (Kaehler, et al. 2011) for nonprismatic member design calculations. AASHTO (2017) does have some discussion on how to calculate the LTB capacity of nonprismatic members, but it takes a highly conservative approach. Based on the ease of implementation of its framework, this paper follows and extends the approach laid out in Design Guide 25. In this approach, the elastic buckling capacity of general nonprismatic I-section members is estimated by effectively using an equivalent prismatic member. This capacity is then mapped to an appropriate LTB design resistance. The elastic LTB capacity of the equivalent

doubly- or singly-symmetric prismatic member is calculated using the following fundamental equation for a doubly symmetric I-section member (White and Jung 2003):

$$F_e = \frac{C_b \pi^2 E}{(L_b/r_t)^2} \sqrt{1 + \frac{0.078}{X^2} (L_b/r_t)^2} \quad (1)$$

where  $F_e$  is the theoretical elastic LTB strength in terms of stress,  $C_b$  is the moment gradient modifier, defined and discussed in the next section,  $E$  is the modulus of elasticity,  $L_b$  is the length between points that are either braced against lateral displacement of the compression flange or braced against twist of the cross-section, and

$$r_t \cong \frac{b_{fc}}{\sqrt{12 \left( \frac{h}{d} + \frac{1}{3} \frac{A_{wc}}{A_{fc}} \frac{D^2}{hd} \right)}} \quad (2)$$

is the radius of gyration of the compression flange plus one-third of the area of the web in compression. In this equation,  $b_{fc}$  is the width of the flange in compression,  $h$  is the distance between the centroids of each flange,  $D$  is the web depth,  $d$  is the full depth of the section,  $A_{wc}$  is the area of the web in compression, and  $A_{fc}$  is the area of the flange in compression. Additionally, in Eq. 1,

$$X^2 = \frac{S_{xc} h}{J} \quad (3)$$

where  $S_{xc}$  is the elastic section modulus to the outermost fiber in compression and

$$J = \frac{Dt_w^3}{3} + \frac{b_{ft} t_{ft}^3}{3} \left( 1 - 0.63 \frac{t_{ft}}{b_{ft}} \right) + \frac{b_{fc} t_{fc}^3}{3} \left( 1 - 0.63 \frac{t_{fc}}{b_{fc}} \right) \quad (4)$$

is the St. Venant torsional constant of the I-section. Note that if the web is slender  $\left( \frac{h_c}{t_w} > 5.70 \sqrt{\frac{E}{F_{yc}}} \right.$  or  $\left. \frac{I_{yc}}{I_y} \leq 0.23 \right.$  in AISC (2016) and AASHTO (2017) ) at any position along the unbraced length

under consideration,  $J$  is taken equal to zero. The variable  $h_c$  is equal to 2x the distance from the centroid of the cross-section to the inside face of the compression flange,  $t_w$  is the thickness of the web,  $t_{fc}$  and  $t_{ft}$  are the thicknesses of the compression and tension flanges,  $F_{yc}$  is the specified minimum yield strength of the compression flange,  $I_{yc}$  is the moment of inertia of the compression flange about the minor-axis of bending, and  $I_y$  is the moment of inertia of the entire cross-section about the minor-axis of bending.

The equivalent prismatic member is a fictitious member that is the same unbraced length as the actual nonprismatic member but has a constant cross-section equal to the cross-section at the

critical location in the nonprismatic member (for calculation of the elastic LTB capacity). Determination of the critical location is essential to obtain the best estimate of the buckling capacity on the nonprismatic member. AASHTO (2017) conservatively uses the location where  $r_t$  is smallest as the critical location and forces  $C_b$  to be taken as 1.0. Recommendations are discussed in this paper to improve upon this current AASHTO procedure. The next section discusses the definition of the critical location for the elastic LTB calculation adopted in the first and second editions of Design Guide 25 (Kaehler et al. 2011; White and Jeong 2019).

### 3. Efficient manual calculations for nonprismatic I-section members

Efficient manual calculations can be achieved for nonprismatic I-section members by a straightforward adaptation of the AISC (2016) and/or AASHTO (2017) provisions for prismatic I-section members. Regarding the LTB limit state, the equations can be configured so that the engineer needs to focus only on the calculation of:

- 1) The elastic lateral-torsional-buckling load ratio,  $\gamma_e$ , which is the ratio of the load level at theoretical elastic buckling to the required design load level, and
- 2)  $F_{nc}$  at the cross-section with the largest  $f_{bu}/F_{nc}$  at any cross-section along the unbraced length under consideration for slender-web, or  $M_u/M_{nc}$  for nonslender-web I-section members, where  $f_{bu}$  is the factored compressive stress in the flange under consideration,  $M_u$  is the factored moment and  $M_{nc}$  is the nominal moment capacity.

In addition, the member capacities may be limited by cross-section based limit states checks.

#### 3.1 Manual estimate of $\gamma_e$

The elastic LTB strength of a general nonprismatic member may be estimated as

$$\gamma_e = \frac{C_b}{\left(\frac{f_{bu}}{F_{e1}}\right)_{\max}} \quad (5)$$

where  $(f_{bu}/F_{e1})_{\max}$  is the maximum ratio of the factored compression flange major-axis bending stress to the elastic lateral-torsional-buckling stress (the location corresponding to  $(f_{bu}/F_{e1})_{\max}$  is defined as the critical location for the elastic LTB calculation),  $F_{e1}$  is the reference elastic buckling stress for the location under consideration, determined from Eq. 1 using  $C_b = 1$ , the compression flange stress,  $f_{bu}$ , is calculated from the moment diagram under consideration, and the recommended moment gradient factor is

$$C_b = \frac{4 \left(\frac{f_{bu}}{F_{e1}}\right)_{\max} \chi}{\sqrt{\left(\frac{f_{bu}}{F_{e1}}\right)_{\max}^2 + 4 \left(\frac{f_{bu}}{F_{e1}}\right)_A^2 + 7 \left(\frac{f_{bu}}{F_{e1}}\right)_B^2 + 4 \left(\frac{f_{bu}}{F_{e1}}\right)_C^2}} \quad (6)$$

where  $\chi$  is the nonprismatic geometry factor discussed in Section 4, and the subscripts A, B, C, and max represent the quarter point values at 25% of  $L_b$ , 50% of  $L_b$ , 75% of  $L_b$ , and the maximum value, respectively.

Note that the ratios in Eqs. 5 and 6 can be expressed in terms of moments instead of stresses since both the bending stress and buckling stress are with respect to the compression flange at the same location. Also in the limit of a prismatic doubly symmetric member subjected to any moment diagram, or a prismatic singly symmetric member under single-curvature bending, the buckling capacity  $F_{e1}$  is constant along the length and Eq. 5 reduces to Equation C-F1-2b of the AISC *Specification* recommended by Wong and Driver (2010),

$$C_b = \frac{4M_{\max}}{\sqrt{M_{\max}^2 + 4M_A^2 + 7M_B^2 + 4M_C^2}} \quad (7)$$

The Wong and Driver (2010) quarter point formula is recommended instead of the AISC (2016) quarter point formula or the AASHTO (2017) formula for the calculation of  $C_b$ . Benefits relative to the AISC equation are a general improvement in the mean and coefficient of variation relative to analytical results, as well as a more accurate lower-bound fit to analytical results for linear moment gradient cases. Benefits over the AASHTO equation are significantly greater accuracy for nonlinear moment diagrams when the largest bending occurs within the unbraced length. Note that the results from this paper also indicate that there is no need for a cap on the  $C_b$  in Eqs. 6 and 7. A rigorous evaluation of each of the above approaches is given in Slein et al. (2018).

### 3.2.a Flexural capacity of slender-web members in Design Guide 25

To estimate the nominal LTB resistance,  $F_{nc}$ , for any slender-web nonprismatic members (in terms of compression flange stress), the following steps are recommended:

- 1) For a given nonprismatic unbraced length, determine the buckling load ratio,  $\gamma_e$ .
- 2) Calculate  $F_L$ .
- 3) Use  $\gamma_e$  and  $F_L$  to map from the elastic LTB resistance to the LTB design resistance.
- 4) Take the LTB design resistance as the  $F_{nc}$  at the critical cross-section for strength where  $f_{bu}/F_{nc}$  is maximum.

#### Step 1

The buckling load ratio,  $\gamma_e$ , can be determined directly as the eigenvalue from an elastic buckling analysis or can be estimated manually using Eq. 5. Note that  $\gamma_e$  characterizes the buckling behavior of the entire unbraced length, and therefore only needs to be calculated once, at the critical location where  $(f_{bu}/F_{e1})$  is maximum. Once  $\gamma_e$  is known, the remaining calculations focus on the critical cross-section for strength.

#### Step 2

The value

$$F_L = 0.5F_{yc} \quad (8)$$

is recommended.

#### Step 3

Map the elastic buckling resistance to the nominal LTB design resistance for the member using the buckling curve in the AISC and AASHTO *Specifications*. (The coefficient of 0.8 below is recommended for the compact limit anchor point for general welded sections; 1.1 is recommended

in place of 0.8 as the compact limit anchor point for rolled sections and for doubly-symmetric welded sections with  $D/b_{fc} < 3$ .)

For  $\frac{\gamma_e f_{bu}}{F_{yc}} \geq \frac{\pi^2}{0.8^2} = 15.4$ , the lateral-torsional buckling limit state does not apply.

For  $15.4 > \frac{\gamma_e f_{bu}}{F_{yc}} > \frac{F_L}{F_{yc}}$ ,

$$F_{nc} = R_{pg} R_{pc} \frac{M_{yc}}{S_{xc}} \left[ 1 - \left( 1 - \frac{F_L}{R_{pc} F_{yc}} \right) \left( \frac{\pi \sqrt{\frac{F_{yc}}{\gamma_e f_{bu}} - 0.8}}{\pi \sqrt{\frac{F_{yc}}{F_L} - 0.8}} \right) \right] \leq R_{pg} R_{pc} \frac{M_{yc}}{S_{xc}} \quad (9)$$

For  $\frac{\gamma_e f_{bu}}{F_{yc}} \leq \frac{F_L}{F_{yc}}$ ,

$$F_{nc} = R_{pg} \gamma_e f_{bu} \quad (10)$$

where  $R_{pg}$  is the web bend-buckling strength reduction factor (denoted by  $R_b$  in AASHTO (2017)).

### 3.2.b Flexural capacity of compact and noncompact web members in Design Guide 25

To estimate the nominal LTB resistance,  $F_{nc}$ , for any compact and noncompact web nonprismatic members, follow the steps in 3.2.a with the following changes to Step 2.

#### Step 2

For welded I-section members, it is recommended that  $F_L$  be taken as  $0.5F_y$  as stated in Eq. 8.

For rolled I-section members, which all have compact webs and are of course prismatic,

$$F_L = 0.7F_y \quad (11)$$

### 3.2.c Flexural capacity of slender-web members in proposed AASHTO Specifications

To estimate the nominal LTB resistance,  $F_{nc}$ , for any slender-web nonprismatic members (in terms of compression flange stress), the following steps are recommended:

- 1) For a given nonprismatic unbraced length, determine the buckling load ratio,  $\gamma_e$ .
- 2) Determine an equivalent  $r_t$ .
- 3) Use the equivalent  $r_t$  to map from the elastic LTB resistance to the LTB design resistance at the critical cross-section for strength, defined where  $f_{bu}/R_h F_{yc}$  is largest, where  $R_h$  is the hybrid factor.

#### Step 1

The buckling load ratio,  $\gamma_e$ , can be determined as stated in Step 1 of Section 3.2.a.

*Step 2*

Note that it is useful to define an equivalent  $r_t$  equation in terms of  $\gamma_e$ . This allows the direct use of the *Specification* inelastic LTB equation, which is written in terms of lengths, to be employed for nonprismatic members. This is the approach taken in proposed AASHTO LRFD provisions.

The buckling load ratio,  $\gamma_e$ , is a single constant value that applies to the entire unbraced length. Therefore, the elastic buckling stress at any location along the length of the member may be expressed as,

$$F_e = \gamma_e f_{bu} \quad (12)$$

Taking Eq. 1 with  $C_b = 1$  (the moment gradient effects are handled via  $\gamma_e$ ) and  $J = 0$ , for slender-web members, and solving for  $r_t$

$$r_t = \frac{L_b}{\pi} \sqrt{\frac{F_e}{E}} \quad (13)$$

This is an “equivalent”  $r_t$ , which can be substituted into the LTB equations to connect into the framework of the AISC and AASHTO LTB equations, and allows the provisions to map from  $F_e$  in Eq. 12 to the nominal resistance,  $F_{nc}$ , based on the unbraced length. The equivalent  $r_t$  from Eq. 13 can be substituted into the standard AISC and AASHTO equations for the anchor points of the LTB curve to perform the LTB calculations. This substitution is shown algebraically in the following to demonstrate the equivalency compared to the Design Guide 25 approach:

$$L_p = 0.8 r_t \sqrt{\frac{E}{F_{yc}}} = \frac{0.8}{\pi} L_b \sqrt{\frac{F_e}{F_{yc}}} \quad (14)$$

and

$$L_r = \pi r_t \sqrt{\frac{E}{F_{yr}}} = L_b \sqrt{\frac{F_e}{F_{yr}}} \quad (15)$$

The variable  $L_p$  is the limiting unbraced length to achieve the nominal flexural resistance of  $R_b R_h F_{yc}$ . The coefficient of 0.8 in Eq. 14 applies generally to welded I-sections; Appendix A6 of the proposed AASHTO provisions specifies an  $L_p$  coefficient of 1.1 for rolled sections and doubly symmetric welded sections with  $D/b_{fc} \leq 3.0$ . The variable  $L_r$  is the limiting unbraced length to achieve the onset of nominal yielding in either flange, with consideration of compression-flange residual stress effects. The term  $F_{yr}$  is the compression-flange stress at the onset of nominal yielding within the cross-section including residual stress and geometric imperfection effects (analogous to  $F_L$  in AISC (2016) and White and Jeong (2019)), taken as  $0.5F_{yc}$  for welded sections and  $0.7F_{yc}$  for rolled sections. For inelastic LTB, the equivalency of the use of Eq. 13 for  $r_t$  to the Design Guide 25 approach involving the direct use of  $\gamma_e$  and  $F_L$  can be verified by substituting the

limiting lengths from Eqs. 14 and 15 into  $\frac{L_b - L_p}{L_r - L_p}$  :

$$\begin{aligned}
\frac{L_b - L_p}{L_r - L_p} &= \frac{L_b - 0.8r_t \sqrt{\frac{E}{F_y}}}{\pi r_t \sqrt{\frac{E}{F_{yr}}} - 0.8r_t \sqrt{\frac{E}{F_y}}} = \frac{L_b - 0.8 \left( \frac{L_b}{\pi} \sqrt{\frac{F_e}{E}} \right) \sqrt{\frac{E}{F_y}}}{\pi \left( \frac{L_b}{\pi} \sqrt{\frac{F_e}{E}} \right) \sqrt{\frac{E}{F_{yr}}} - 0.8 \left( \frac{L_b}{\pi} \sqrt{\frac{F_e}{E}} \right) \sqrt{\frac{E}{F_y}}} \\
&= \frac{1 - \frac{0.8}{\pi} \sqrt{\frac{F_e}{F_y}}}{\sqrt{\frac{F_e}{F_{yr}}} - \frac{0.8}{\pi} \sqrt{\frac{F_e}{F_y}}} = \frac{\pi \sqrt{\frac{F_y}{F_e}} - 0.8}{\pi \sqrt{\frac{F_y}{F_{yr}}} - 0.8}
\end{aligned} \tag{16}$$

This is the same as the corresponding portion of Eq. 9.

### Step 3

As a conservative approximation, the smallest  $R_b$  at any cross-section within the unbraced length is used throughout to simplify the identification of the critical cross-section for the strength calculation where  $f_{bu}/R_h F_{yc}$  is maximum. Without this simplification,  $f_{bu}/F_{nc}$  generally needs to be calculated at several cross-sections to determine the location of the critical cross-section for strength.

One maps the elastic buckling resistance to the nominal LTB design resistance for the member using the AISC and AASHTO LTB equations and the limiting unbraced lengths defined by Eqs. 14 and 15.

### 3.2.d Flexural capacity of compact- and noncompact-web members in proposed AASHTO Specifications

To estimate the nominal LTB resistance,  $F_{nc}$ , for any compact- and noncompact-web nonprismatic members, the following steps are recommended:

- 1) For a given nonprismatic unbraced length, determine the buckling load ratio,  $\gamma_e$ .
- 2) Determine an equivalent  $r_t$ .
- 3) Use the equivalent  $r_t$  to map from the elastic LTB resistance to the LTB design resistance at the critical cross-section for strength, defined where  $f_{bu}/R_{pc} F_{yc}$  is largest.

### Step 1

The buckling load ratio,  $\gamma_e$ , can be determined as stated in Step 1 of Section 3.2a.

### Step 2

An equivalent  $r_t$  equation is calculated in a similar manner as Step 2 in Section 3.2c but using Eq. 1 with  $C_b = 1$  (moment gradient effects are handled via  $\gamma_e$ ) and a finite  $J$ . Solving for  $r_t$ , one obtains



$$r_t = \frac{\frac{L_b}{1.95} \frac{F_e}{E}}{\sqrt{\frac{J}{S_{xc} h} + \sqrt{\left(\frac{J}{S_{xc} h}\right)^2 + 6.76 \left(\frac{F_e}{E}\right)^2}}} \quad (17)$$

This is an “equivalent”  $r_t$ , which can be substituted into the LTB equations to connect into the framework of the AISC and AASHTO LTB equations, and allows the provisions to map from  $F_e$  in Eq. 12 to the nominal resistance,  $F_{nc}$ , based on the unbraced length. The equivalent  $r_t$  from Eq. 17 can be substituted into the standard equations for the anchor points of the AISC and AASHTO LTB equations to perform the LTB calculations. This substitution is shown algebraically in the following to demonstrate the equivalency:

$$L_p = 0.8 r_t \sqrt{\frac{E}{F_{yc}}} \quad (18)$$

and

$$L_r = 1.95 r_t \frac{E}{F_{yr}} \sqrt{\frac{J}{S_{xc} h}} \sqrt{1 + \sqrt{1 + 6.76 \left(\frac{F_{yr} S_{xc} h}{E J}\right)^2}} \quad (19)$$

For inelastic LTB, the equivalency of the use of Eq. 17 for  $r_t$  to the Design Guide 25 approach involving the direct use of  $\gamma_e$  and  $F_L$  can be verified by substituting the limiting lengths from Eqs.

18 and 19 into  $\frac{L_b - L_p}{L_r - L_p}$ :

$$\frac{L_b - L_p}{L_r - L_p} = \frac{L_b / r_t - L_p / r_t}{L_r / r_t - L_p / r_t} = \frac{1.95 \frac{E}{F_e} \sqrt{\frac{J}{S_{xc} h}} \sqrt{1 + \sqrt{1 + 6.76 \left(\frac{F_e S_{xc} h}{E J}\right)^2}} - 0.8 \sqrt{\frac{E}{F_{yc}}}}{1.95 \frac{E}{F_{yr}} \sqrt{\frac{J}{S_{xc} h}} \sqrt{1 + \sqrt{1 + 6.76 \left(\frac{F_{yr} S_{xc} h}{E J}\right)^2}} - 0.8 \sqrt{\frac{E}{F_{yc}}}} \quad (20)$$

This is the same as the corresponding portion of Eq. 9.

### Step 3

The critical cross-section for strength is the one where  $f_{bu}/R_{pc}F_{yc}$  is maximum. One maps the elastic buckling resistance to the nominal LTB design resistance for the member following the AISC and AASHTO LTB equations through the limiting unbraced lengths defined by Eqs. 17, 18, and 19.

## 4. Nonprismatic geometry factors

The additional term  $\chi$  in Eq. 6, called the nonprismatic geometry factor, is introduced and applied to the moment gradient modifier to account for stability effects induced by geometric and cross-

section properties that are unrelated to the moment gradient. In the limit that the member becomes prismatic, the nonprismatic geometry factor becomes equal to 1.0.

Note that all of the studies used to derive the nonprismatic geometry factors are based on members with extreme and intermediate cross-section properties within the scope for design laid out in Design Guide 25 (White and Jeong 2019). These members were tested using a full factorial combination of geometric configurations and loadings, totaling several hundred thousand permutations. The development of the nonprismatic geometry factor is based on thin-walled open-section beam theory where every cross-section is modeled perpendicular to the shear center. Limits are established on the application of the resulting equations to avoid unconservative estimates larger than 7 % for the various nonprismatic geometries. Cases near these limits are often sensitive to minor changes in the loading or geometry. It is recommended that a direct buckling analysis be conducted for members that violate these limits.

#### 4.1 Single linear variations in web depth

For members with prismatic flanges and a single linear variation in web depth, the nonprismatic geometry factor is calculated as

$$\chi = 1 + r_I \quad (21)$$

where  $r_I$ , the flange inclination factor, is taken as zero except when  $I_{yP} / I_{yT} \leq 1.0$ ,

$$r_I = \min \left[ 0.0, -0.02|\beta| \left( 1 - \frac{1}{I_{yT} / I_{yP}} \right) \right] \quad (22)$$

In this equation,  $\beta$  is the taper angle between the flanges of the I-section, expressed in degrees,  $I_{yP}$  is the moment of inertia about the y-axis of the flange perpendicular to the axis about which twisting is restrained at the braced points (referred to as the non-tapered flange), and  $I_{yT}$  is the moment of inertia about the y-axis for the flange attached to the tapered edge of the I-section web (referred to as the tapered flange). Note that the coefficient 0.02 in Eq. 22 converts the taper angle from degrees to radians and that  $\beta$  is limited to a maximum of 15 degrees. The flange inclination factor,  $r_I$ , is applicable to any nonprismatic section with a shear center axis that does not have the same orientation as the axis of the torsional constraint at the braced points. When  $I_{yT}$  is greater than  $I_{yP}$ , the elastic LTB resistance tends to be reduced measurably as the taper angle increases. It is important to note that this stability effect is observed regardless of which flange is in compression. Fig. 1 shows the influence of flange size on the inclination of the shear center.

If both flanges have an equal taper angle with respect to the axis of the torsional restraints,  $\chi$  should be taken equal to 1.0. If both flanges are tapered at an unequal angle with respect to the axis of the torsional restraints, conservatively take the flange with the smaller moment of inertia about the y-axis as the flange perpendicular to the torsional restraint in calculating  $I_{yP}$ . The nonprismatic geometry factor accounts for the differences in the orientation of the shear center axis and the axis about which the twist is constrained at the braced points, since a large  $I_{yT}/I_{yP}$  corresponds to a larger angle of the shear center relative to the axis about which twist is constrained. Any other bracing effects should be handled with additional modifications to the LTB capacity.

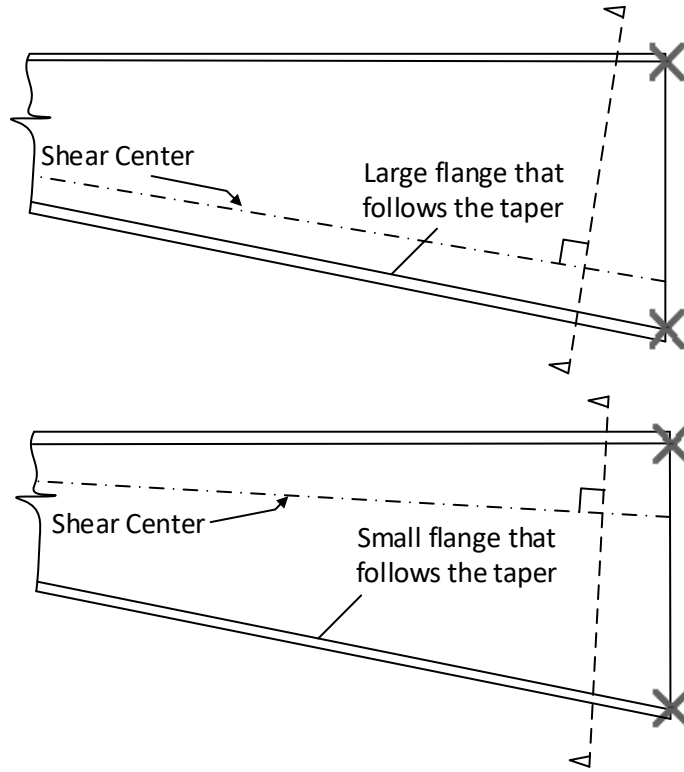


Figure 1: Example orientations of the shear center for a section with a large flange that follows the web taper (top) and a section with a small flange that follows the web taper (bottom).

#### 4.2 Double linear variations in web depth

For members with prismatic flanges and two linear variations in the web depth within the unbraced length, the nonprismatic geometry factor is calculated by Eq. 23a for single-curvature bending and Eq. 23b for reverse-curvature bending:

$$\chi = 1 + r_l + r_{DT} + r_k \quad (23a)$$

$$\chi = 1 + r_l + r_{DT} + r_k \leq 1.0 \quad (23b)$$

where  $r_l$ , the flange inclination factor, is defined from Eq. 22 with  $\beta$  defined as the flange taper angle with the largest magnitude. The double taper factor,  $r_{DT}$ , is defined as

$$r_{DT} = 0.02 \left( \frac{L_1}{L_b} \right) (\beta_1 + \beta_2) \left( 1 - \frac{h_{\min}}{h_{\max}} \right)^2 \quad (24)$$

where  $L_1$  is the shorter of the two linearly tapered lengths within the design segment,  $\beta_1$  is the taper angle between the flanges in the shorter of the two linearly tapered lengths, taken as positive when the web depth decreases in the direction moving along the length from the end of the unbraced length under consideration, expressed in degrees,  $\beta_2$  is the taper angle between the flanges in the longer of the two linearly tapered lengths, taken as positive when the web depth decreases in the

direction moving along the length from the end of the unbraced length, expressed in degrees,  $h_{min}$  is the minimum web depth within the unbraced length, and  $h_{max}$  is the maximum web depth within the unbraced length. Note that for reverse-curvature bending,  $\chi$  is not allowed to be greater than 1.0. Figure 2 illustrates a number of the above variables.

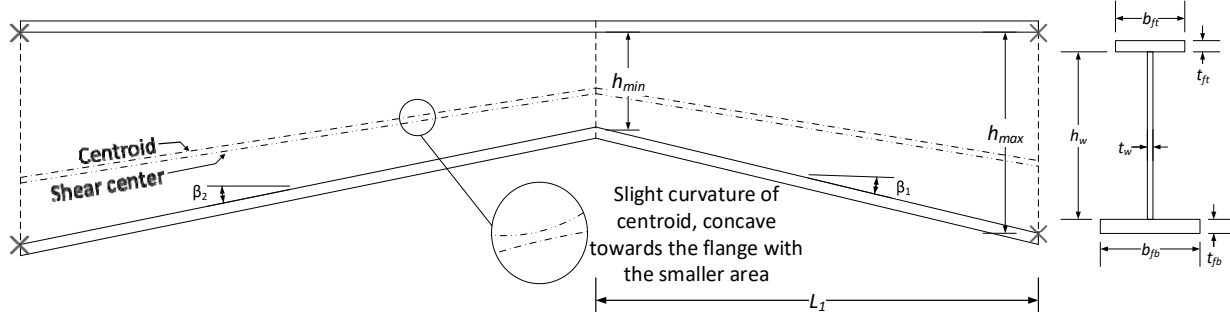


Figure 2: Example “kinked-in” member.

The double taper factor,  $r_{DT}$ , accounts for the deviation of the cross-section shear center from a straight line within the unbraced length and the “kinked” geometry of the doubly-tapered flange. This factor is positive when the tapered flange is “kinked-in,” i.e., when  $\beta_1 + \beta_2$  is positive, and it is negative when the tapered flange is “kinked-out,” i.e., when  $\beta_1 + \beta_2$  is negative. This factor has a larger magnitude for smaller  $h_{min} / h_{max}$  and it is largest when the pinch point is located at the middle of the unbraced length, i.e., when  $L_1/L_b = 0.5$ . In the limit that  $L_1/L_b$  approaches zero, the design segment is linearly tapered and  $r_{DT}$  approaches zero.

The kinked-out flange factor,  $r_K$ , is zero if  $\beta_1 + \beta_2$  is greater than or equal to zero; otherwise  $r_K$  is defined by Eq. 25a for unbraced lengths subject to single-curvature bending causing compression in the non-tapered flange, and for all other cases  $r_K$  is defined by Eq. 25b:

$$r_K = \min [0, 0.02(\beta_1 + \beta_2)] \quad (25a)$$

$$r_K = \min [0, 0.06(\beta_1 + \beta_2)] \quad (25b)$$

The kinked-out flange factor,  $r_K$ , captures an additional strength reduction encountered when the depth is “kinked-out” within the unbraced length, i.e., when the sum of  $\beta_1$  and  $\beta_2$  is negative. In the limit that  $\beta_1$  approaches  $\beta_2$ , the design segment is linearly tapered and  $r_K$  approaches zero. The combination of Eqs. 24 and 25 capture “arch” and “inverted arch” effects in the doubly tapered member. The arch effect is the tendency of a member to be less stable out-of-plane for bending that tends to open the arch. Equation 24 is influenced by: (1) the relationship between the taper angles  $\beta_1$  and  $\beta_2$ , where larger angles of the same sign indicate a deeper “arch.”; (2) the location of the kink, where a kink location at midspan results in the greatest effect; and (3) the ratio of the minimum and maximum web height in the span. These parameters describe the shape of the so-called arch. Furthermore, the use of Eq. 25a or 25b is a function of which flange is in compression for kinked-out cases.

Note that the  $\chi$  factor given by Eqs. 23a and 23b is applicable for  $\beta_1$  and  $\beta_2$  of -15 to 15 degrees if the sum of  $\beta_1$  and  $\beta_2$  is greater than or equal to zero; otherwise  $\beta_1$  and  $\beta_2$  are limited to -5 to 15 degrees. Additionally,  $h_{min}/h_{max}$  must be greater than or equal to 0.1.

#### 4.3 Concave parabolic haunches

For members with prismatic flanges and any variation in web depth, such that the web depth is continuously increasing, or decreasing, along the unbraced length, and such that the web depth is always less than or equal to the depth from the top of the web to a chord drawn between points at the bottom of the web at the ends of the tapered portion of the unbraced length, the LTB capacity can be accurately to conservatively estimated using the methods in Section 3 and using Eq. 21 as the  $\chi$  factor, where  $\beta$  in Eq. 22 is taken as the chord angle. Figure 3 shows an example of this type of unbraced length.

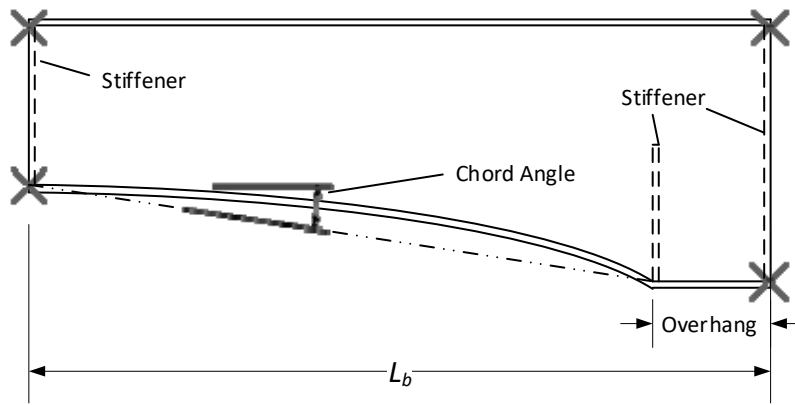


Figure 3: Example concave parabolic haunch member with an overhang.

A concave parabolic haunch experiences a similar flange inclination effect as a single linear variation in web depth. While there will be some difference in behavior associated with these variations in the web depth, the  $\chi$  factor can be calculated simply using Eq. 21. Potential unconservative predictions from this simplification are mitigated by not relying on the largely beneficial inverted arch effects. For unbraced lengths in parabolic haunches, the maximum chord angle allowed is 10 degrees. This is because the tangent angle of the bottom flange at one end, or at a “kink point” such as that shown at the end of an overhang as shown in Fig. 3, will tend be larger than the chord angle. Additional restrictions include limiting the overhang length to a maximum of  $0.2L_b$  and including at least a half-depth bearing stiffener at the kink (placing a stiffener at the kink has also been recommended by Sause et al. 2017).

#### 4.4 Steps in cross-section

To estimate the LTB capacity of members that have a step in the cross-section within the unbraced length, follow the methods laid out in Section 3 but modify Eq. 6 as follows:

If there are one or more steps within the quarter-lengths adjacent to point A,

Take  $F_{el}$  in  $\left( \frac{f_{bu}}{F_{el}} \right)_A$  as the minimum buckling capacity for the cross-sections within 0 to  $0.5L_b$ .

If there are one or more steps within the quarter-lengths adjacent to point B,

Take  $F_{e1}$  in  $\left(\frac{f_{bu}}{F_{e1}}\right)_B$  as the minimum buckling capacity within  $0.25L_b$  to  $0.75L_b$ .

If there are one or more steps within the quarter-lengths adjacent to point C,

Take  $F_{e1}$  in  $\left(\frac{f_{bu}}{F_{e1}}\right)_C$  as the minimum buckling capacity within  $0.5L_b$  to  $L_b$ .

This modification accounts for the lack of resolution of the quarter point formula, i.e., the quarter point formula samples the  $f_{bu}/F_{e1}$  values at only a maximum of four points, only at three points when the maximum value is at A, B or C. Additionally, if the member has a cross-section step as well as a variable web depth, the modification to Eq. 6 along with the appropriate  $\chi$  factor gives an accurate to conservative estimate of the LTB capacity. Note that since both methods individually give accurate to conservative results, there is potential for estimations to be more conservative for extreme cases. Additionally steps in the cross-section are limited to a change in the lateral moment of inertia of the flanges of no more than a factor of 2.0 at any step, and adjacent steps closer than 25 % of the unbraced length are considered as one step and the total change in the lateral moment of inertia may not exceed 2.0 for these steps.

Members with a stepped cross-section such that: 1)  $D_{cL}/D_{cS} \geq 1.2$ , where  $D_{cL}$  is the depth of the web in compression at the section with the larger gross area and  $D_{cS}$  is the depth of the web in compression at the section with the smaller gross area; and 2) the section with the smaller gross area makes up more than 50% of the unbraced length, tend to have a significant reduction in the physical member capacity due the shift of the cross-section centroid at the step. This physical reduction in member capacity is illustrated in Fig. 4, which shows the influence of  $L_{step}/L_b$  on  $\gamma_e$ . It is important to note that to obtain  $D_{cL}/D_{cS} > 1.2$ , the step usually would be only in one flange and the change in the flange lateral moment of inertia would be close to the maximum allowed factor of 2.0.

## 5. Illustration of predictions

The development of the nonprismatic geometry factors ( $\chi$ ), and the validation of the recommended methods, have been conducted using the linear elastic eigenvalue buckling analysis capabilities of the software SABRE2 V2 (White et al. 2019). The reader is referred to Slein and White (2019a and 2019b) for the details of these studies. The following sub-sections present three example calculations and the comparison of the results to experimental and/or refined finite element values.

### 5.1 Studies of members with a double-linear variation in web depth

Yang and Yau (1987) and numerous other researchers have shown that modeling a tapered web I-section member using multiple prismatic finite elements does not give accurate predictions. The FEM package SABRE2 (White et al. 2019), used in this paper addresses both continuously varying member tapers as well as discrete steps in the cross-section geometry. To demonstrate the issue identified by Yang and Yau, the predictions for various flexurally and torsionally simply supported members with a double linear variation in their web depth are compared to converged elastic shell linear buckling solutions performed by Jeong (2014). The members are loaded at midspan by a transverse point load applied at the shear center. The section is doubly symmetric so the shear center and the mid-depth of the web are at the same height; therefore, there is theoretically no load height effect. Three different variations of these members are considered by defining the “design

axis” (i.e., a straight reference line from which the cross sections are defined) at the top of the web, the web mid-depth, and the bottom of the web (see Fig. 5). In all of the cases studied, the web depth,  $d_w$ , varies from 24 in. at midspan to a depth ranging from 24 in. to 2.4 in. at the simply-supported member ends. The variable  $\alpha$ , is the ratio of the depth at the member ends to the depth at the midspan. The suite of member  $\alpha$  values and corresponding end web depths studied are shown in Table 1.

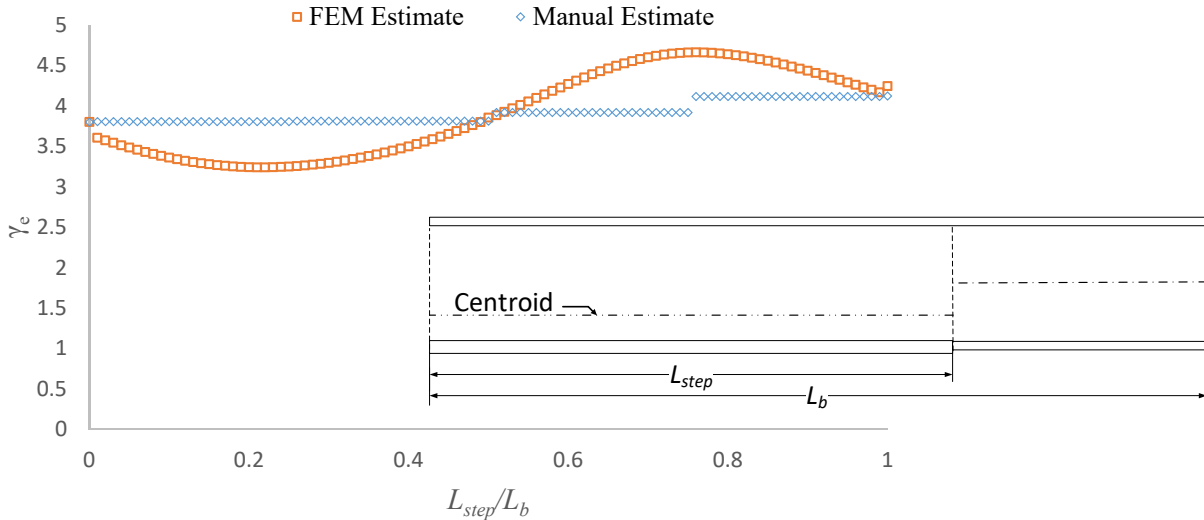


Figure 4: Example FEM and manual estimates of  $\gamma_e$  for a representative stepped unbraced length with  $D_{cL}/D_{cS} \geq 1.2$  at the step, such that the recommended calculations are not applicable.

Figure 6 shows that the capacities of the variable web depth members are a function of the location of the design axis, where the kinked-out members with compression in the non-tapered flange (design axis at the top of the web) tend to have larger capacity than kinked-out members with compression in the tapered flange (design axis at the web mid-depth and at the bottom of the web). Following the rules laid out in Section 4.2,  $\beta$  is limited to -5 degrees in the manual calculations, which use Eqs. 25a and 25b. For  $\alpha = 1.0$  (prismatic members), the quarter point formula, Eq. 7, gives  $C_b = 1.26$ . The rigorous SABRE2 and shell FEM elastic buckling solutions correspond to a  $C_b$  of 1.36 for the specific prismatic case studied in this example.

One can observe that the SABRE2 and elastic shell FEM solutions match very closely. The manual estimates for this problem follow the trend that larger strengths are obtained for members with the design axis at the top of the web (i.e., with the non-tapered flange in compression), and smaller strengths with the design axis at the web mid-depth or at the bottom of the web (i.e., with both flanges equally tapered or with the tapered flange in compression). The manual estimate predicts the same capacity for the cases with the design axis at the web mid-depth and at the bottom of the web. The manual estimates for this problem are increasingly conservative for smaller  $\alpha$  (i.e., larger taper).

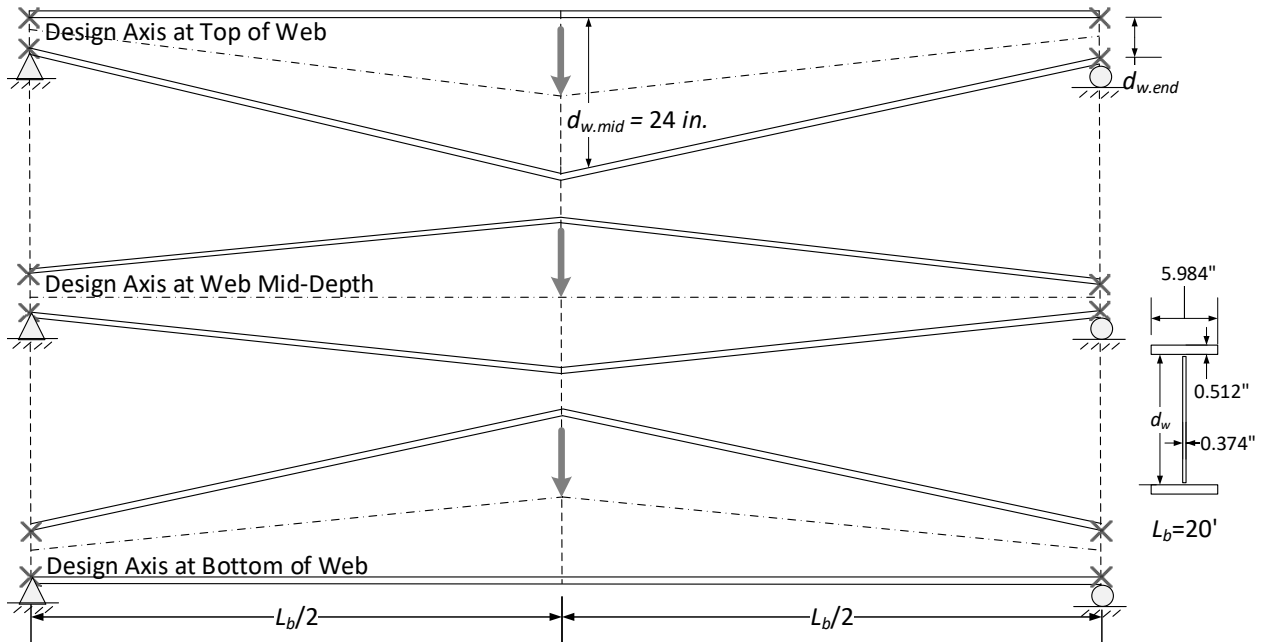


Figure 5: Example torsionally simply-supported members with a double linear variation in web depth, with three different design axes and different values of  $\alpha = d_{w,end}/d_{w,mid}$  (refined solutions for design axis at the web mid-depth provided by Yang and Yau (1987), elastic shell buckling analysis solutions for all cases provided by Jeong (2014).

Table 1: Web depths at each end of the member as a function of  $\alpha$ .

$\alpha$	0.1	0.15	0.2	0.3	0.4	0.5	0.6	0.7	0.8	0.9	1
$d_w$ at ends (in)	2.4	3.6	4.8	7.2	9.6	12	14.4	16.8	19.2	21.6	24

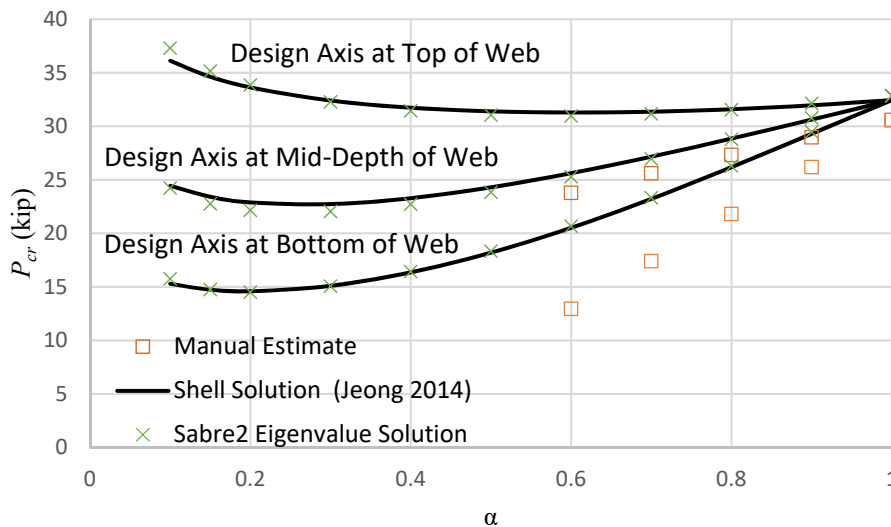


Figure 6: Comparison of SABRE2 solution and manual estimates to converged shell solutions.

### 5.2 I-girder with a parabolic haunch and a step in the cross-section

To demonstrate the calculation of the capacity of an I-girder with a variable web depth plus a step in the cross-section, a detailed calculation is given for an as-built haunched bridge girder. This



example looks at the pre-retrofit segment 1 of the Harrison Avenue bridge in Scranton PA, described by Sause et al. (2017). The girder properties are listed in Table 2 and an elevation view is shown in Fig. 7 below; the subscript left describes the properties at the left end of the girder, right describes the right end, and the absence of any directional subscript means that dimension is constant along the unbraced length.

Table 2: Girder properties for segment 1 of the Harrison Avenue bridge (units are in inches unless noted otherwise)

$b_{fb}$	$t_{fb\_left}$	$t_{fb\_right}$	$b_{ft}$	$t_{ft\_left}$	$t_{ft\_right}$	$t_w$	$L_b$ (ft)	$L_{step}$	$\beta_{chord}$	$h_{left}$	$h_{right}$
18	1.375	2	18	1	1.375	0.813	21.667	$0.688L_b$	1.866	54.412	62.881

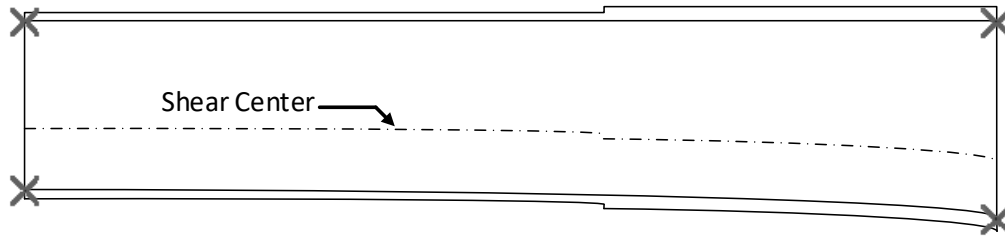


Figure 7: Elevation view of pre-retrofit segment 1 of the Harrison Avenue bridge. Not drawn to scale.

The girder unbraced length shown in Fig. 7 is evaluated under specified internal moments of 74,676 kip-in and of 137,844 kip-in at its left and right ends, respectively, from Sause et al. (2017). Additional internal moments reported at several stations within the unbraced length indicate a close to linear moment diagram. Table 3 shows the manual  $\gamma_e$  with the modifications to  $C_b$  for stepped members defined in Section 4.4 and the appropriate  $\chi$  factor approximating the effect of the flange inclination of this concave parabolic haunch as a single linear variation in web depth. Table 4 illustrates the mapping of the member strength to the nominal capacity using Section 3.2d assuming 50 ksi yield strength. The result is conservative relative to Sause et al. (2017), but is significantly larger than the estimate by the current AASHTO (2017) approach. The SABRE2 solution predicts that the member is governed by lateral-torsional buckling.

Table 3: Comparison of manual estimate of  $\gamma_e$  to FEM calculation of  $\gamma_e$ , segment 1 of the Harrison Avenue bridge.

Manual Estimate								AASHTO (2017)	$\gamma_e$ FEM
$C_b$ w/o $\chi$ & w/o mod. for step	$(f_{bu}/F_{el})_{max}$	$C_b$ w/o $\chi$ & w/ mod. for step	$I_{yp}/I_{yT}$	$\beta_{chord}$	$\chi$	$C_b$ w/ $\chi$ & mod. for step	$\gamma_e$	$\gamma_e$	SABRE2
1.146	0.686	1.141	0.727	1.866	0.990	1.129	1.65	1.46	1.71

Table 4: Manual vs FEM nominal capacity, segment 1 of the Harrison Avenue bridge (units in kips and inch).

Manual Estimate at Station 100.67							$M_n$ FEM at Station 100.67	
$A_{rs}^1$	Composite $S_{xc}^2$	$R_{pc}$	$r_t$	$L_p$	$L_r$	$M_n$	SABRE2 <sup>3</sup>	Sause et al. (2017) <sup>4</sup>
10.7	1918	1.194	4.942	95.2	560.8	95351	87922	96423

1. The area of reinforcing steel was back-calculated given the reported  $S_{xc}$  at Station 100.67.
2. Determined through AASHTO LRFD Appendix D6.2.3. With an assumed factored permanent load applied before the concrete deck equal to 1/3 of the demand at Station 100.67.
3. Equivalent linearly tapered flange thicknesses are used to model the reinforcing steel. These are back-calculated to match the reported  $S_{xc}$  at Stations 86.67, 101.5L, 101.5R, and 108.33. This  $\gamma_e$  solution is intended as an approximate check, since SABRE2 does not address the specific features of the composite I-girder response.
4. Moment at Station 100.67 obtained from a shell nonlinear FEA simulation.

### 5.3 Single linear variation in web depth, experimental test

An important attribute of the proposed methods is that they are based on the idealization of zero flange lateral bending and warping restraint at the ends of the unbraced lengths. Therefore all the manual calculations, and the corresponding estimates from SABRE2 (White et al. 2019) in this paper, are conducted considering only the critical unbraced length, denoted by CS in Fig. 8, except as noted below. Smith et al. (2013) show experimental results for a number of nonprismatic I-section members. These test results may be employed to evaluate the performance of the proposed methods. Test CF1 (Fig. 8) is selected for illustration since it is a singly-symmetric section.

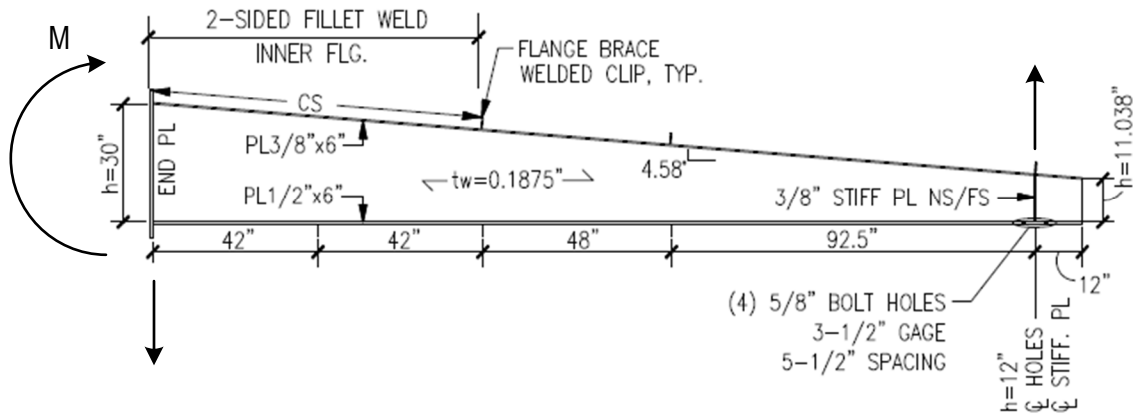


Figure 8: Elevation view of specimen for test CF1, single linear web taper, adapted from Smith et al. (2013).

Smith et al. (2013) state, “Initial lateral-torsional buckling (LTB) of the inner flange occurred within the CS during the first positive cycle of 3% DR ... with a moment at the end-plate of 5,606 kip-in.” The corresponding moments in the CS, are used to evaluate  $\gamma_e$  as shown in Table 5.

Table 5: Comparison of manual estimate of  $\gamma_e M_u$  to FEM calculation of  $\gamma_e M_u$ , test CF1.

Manual Estimate						$\gamma_e M_u$ FEM	
$C_b$	$(f_{bu}/F_{e1})_{max}$	$I_{yp}/I_{yT}$	$\beta$ (degree)	$\chi$	$\gamma_e M_u$	SABRE2	Smith et al.
1.08	0.438	1.33	4.584	1.00	9001	9294	9085

From coupon tests, the respective yield stresses of the top flange, web, and bottom flange are 62.5, 61.9, and 60.0 ksi. Intermediate and final results from the manual procedures discussed in Section 3.2a are compared to several refined inelastic analysis solutions in Table 6.

Table 6: Comparison of manual estimate of  $M_n$  to full nonlinear shell FEM test simulation and an Inelastic Nonlinear Buckling Analysis (INBA) for nominal capacity, test CF1 (all units are in kips and inches).

Manual Estimate						$M_n$ Shell FEM Simulation (Smith et al. 2013)	SABRE2 INBA
$R_{pg}$	$R_{pc}$	$\gamma_e f_{bu}/F_{yc}$	$(\pi/0.8)^2$	$F_L/F_{yc}$	$M_n$		
0.903	1.000	1.456	15.4	0.5	4201	4737	4467

It should be emphasized that the manual and FEM solutions shown in Tables 5 and 6 do not consider any continuity effects with the adjacent unbraced length at the braced point locations, nor lateral bending and warping restraint at the end plate. It is common practice to neglect the influence of effects in routine design, since manual accounting for these effects is relatively difficult.

Consideration of end restraint effects can result in additional predicted capacities when the flexural resistance is governed by LTB, and when significant end restraint effects exist, as discussed by Smith et al. (2013) and White and Jeong (2019). One large benefit of the recommended procedures is that  $\gamma_e$  can be calculated, via a refined elastic LTB analysis based on thin-walled open-section beam theory that captures the end restraint effects. This refined  $\gamma_e$  can be inserted into the equations to map to the nominal resistance of the member. Modeling these effects via SABRE2 (White et al. 2019), the  $\gamma_e M_u$  value is increased to 22,820 kip-in and the mapped nominal moment capacity is increased to 4,943 kip-in. Smith et al. (2013) report similar results. However, upon considering the use of this type of “high-end” computational solution, it is worthwhile to extend these procedures one step further to the use of Inelastic Nonlinear Buckling Analysis (INBA), which provides a direct rigorous calculation of the nominal member resistances. Toğay et al. (2019) show that the SABRE2 INBA solution, considering continuity effects and the additional restraint at the end plate, gives  $M_n = 5,333$  kip-in for CF1. All of these potential routes, of varying complexity, for estimating a nominal member capacity are shown to be accurate to conservative with respect to the experimental test capacity of 5,606 kip-in from Smith et al. (2013).

## 6. Conclusions

Given the methods presented in this paper, member capacities can be manually estimated through straightforward calculations to give accurate to conservative nominal member capacities for general nonprismatic geometries. The calculations focus on finding the elastic lateral-torsional-buckling load ratio,  $\gamma_e$ , and then mapping the load ratio to the appropriate nominal capacity. This method is intended to be user friendly by allowing the mapping to be conducted either with respect to  $\gamma_e$ , as laid out in Design Guide 25, or with respect member length via the use of an equivalent radius of gyration  $r_t$ . The manual calculations can be conducted either in terms of stress or moments since they work with ratios of the ratio of demand to capacity that are the same whether the responses are expressed in terms of stress or in terms of moment. In the limit that the member approaches a prismatic geometry, the nonprismatic member calculations simplify to established prismatic member calculations.

## Acknowledgments

The authors would like to acknowledge Professor Richard Sause of Lehigh University for his major contributions in identifying the proposed AASHTO approach in this paper involving an equivalent  $r_t$ . The authors would also like to acknowledge Mr. Michael A. Grubb of M.A. Grubb & Associates, LLC, Professor Todd Helwig of the University of Texas, Austin, Dr. Karl Frank, Consultant, Drs. Frank Russo and Tom Murphy of Michael Baker International and Modjeski and Masters, respectively, and Mr. Tom Macioce of PennDOT for their contributions toward achieving clarity and applicability of the proposed AASHTO procedures.

## References

- AASHTO (2017). *AASHTO LRFD Bridge Design Specifications*, 8th Edition, American Association of State and Highway Transportation Officials, Washington, D.C.
- AISC (2016). *Specification for Structural Steel Buildings*, ANSI/AISC 360-16, American Institute of Steel Construction, Chicago, IL.
- Jeong, W.Y. (2014). “Structural Analysis and Optimized Design of General Nonprismatic I-Section Members,” Doctoral Dissertation, Georgia Institute of Technology, 256 pp.

- Kaehler, R., White, D.W. and Kim, Y.D. (2011). *Design of Frames Using Web-Tapered Members, Design Guide 25*, 1<sup>st</sup> Edition, American Institute of Steel Construction Chicago, IL, and Metal Building Manufacturers Association, Cleveland, OH.
- Sause, R., Hodgson, I., Tahmasebi, E. (2017). *Lateral-Torsional Buckling Limit State Check for Haunched Girders*. Presented at the meeting of AASHTO T-14.
- Slein, R., Jeong, W.Y., White, D.W. (2018). "A Critical Evaluation of Moment Gradient ( $C_b$ ) Factor Calculation Procedures for Singly Symmetric I-Section Members," Research Report, School of Civil and Environmental Engineering, Georgia Institute of Technology, Atlanta, GA.
- Slein, R. and White, D.W. (2019a). "Design Estimation of the Lateral-Torsional Buckling Resistance of I-Sections with a Linear Taper in the Web Depth," Research Report, School of Civil and Environmental Engineering, Georgia Institute of Technology, Atlanta, GA.
- Slein, R. and White, D.W. (2019b), "Design Estimation of the Lateral-Torsional Buckling Resistance of Prismatic and Non- Prismatic I-Sections with Cross-Section Transitions," Structural Engineering Mechanics and Materials Report, School of Civil and Environmental Engineering, Georgia Institute of Technology, Atlanta, GA.
- Smith, M. D., Turner, K. A., and Uang, C. (2013). "Cyclic Lateral-Torsional Buckling Experiments on Web-Tapered I-Beams" Stability Session S2, *Structural Stability Research Council Conference*, St. Louis, MO, April.
- Toğay, O., Slein, R. and White, D.W. (2019). "Application of Inelastic Buckling Analysis for Design Assessment of Frames Using Nonprismatic I-section Members," *Proceedings*, Annual Stability Conference, Structural Stability Research Council, St. Louis, MO.
- Yang, Y. B. and Yau, J. D. (1987). "Stability of Beams with Tapered I-Sections" *Journal of Engineering Mechanics*, ASCE, 113:1337-1357.
- White, D.W. and Jeong, W.Y. (2019). *Frame Design Using Nonprismatic Members, Design Guide 25*, 2nd Edition, American Institute of Steel Construction Chicago, IL, and Metal Building Manufacturers Association, Cleveland, OH, dedicated in memory of R. Kaehler and Y.D. Kim (under review).
- White, D.W. and Jung, S.K (2003), "Simplified Lateral-Torsional Buckling Equations for Singly-Symmetric I-Section Members," Structural Engineering, Mechanics and Materials Report No. 03-24b, School of Civil and Environmental Engineering, Georgia Institute of Technology, Atlanta, GA.
- White, D.W., Toğay, O., Slein, R., and Jeong, W.Y. (2019). "SABRE2," <[white.ce.gatech.edu/sabre](http://white.ce.gatech.edu/sabre)> (January 7, 2019).
- Wong, E. and Driver, R. (2010), "Critical Evaluation of Equivalent Moment Factor Procedures for Laterally Unsupported Beams," *Engineering Journal*, AISC, Vol. 47, No. 1, pp. 1-20 and Closure, Vol. 47, No. 4, pp. 281-283.